Bulletin of the Earthquake
Research Institute
Vol. 44 (1966), pp. 779-791

42. *Theoretical Seismograms of Spheroidal Type on the Surface of a Homogeneous Gravitating Spherical Earth.*

By Tatsuo Usami and Yasuo Satô,
Earthquake Research Institute.

(Read May 24, 1966.—Received June 30, 1966.)

1. Introduction

In a continuing series of studies of the fundamental properties of theoretical seismograms related to the torsional and spheroidal oscillations of an elastic sphere, results for the cases of a homogeneous sphere with or without liquid core and of the Gutenberg-Bullen A′ earth model have been presented in previous reports.[1] Until now, the gravitational effect has been neglected in these investigations; the present report is the first of several which will consider the influence of gravity on the periods of the free oscillations, the changes it produces in the resulting phase and group velocities, as well as its effect on the Common Spectrum and the resulting theoretical seismograms.

For this investigation, theoretical seismograms were computed for the surface of a homogeneous gravitating elastic sphere by superposition of the disturbances associated with the spheroidal oscillations. Contributions to the motion which are associated with the fundamental radial mode for colatitudinal order numbers $n=95\sim160$ and those associated with the tenth radial mode ($i=10$) were calculated in addition to those already reported for the case neglecting the effect of gravity. Non-dimensional frequencies, phase and group velocities, the Common Spectrum and theoretical seismograms were calculated and comparisons were made with corresponding quantities for the case without gravity.[2]

Remarkable results of the study of the propagation of spheroidal disturbances on the surface of a homogeneous gravitating elastic sphere include:

1. The non-dimensional frequency for the present case tends toward that for the case neglecting the gravitational effect as the colatitudinal

order number n increases. The discrepancy is noticeable only for smaller n and it practically vanishes for $n \geqq 20 \sim 40$.

2. Gravity makes the non-dimensional frequency for $n=0$ smaller, that for $n \geqq 1$ of the fundamental mode larger and its effect on the other modes depends on the radial mode number i and colatitudinal order number n.

3. The difference between the phase and group velocities for the cases with and without gravity is not very great.

4. The Common Spectrum of the colatitudinal component for the present case differs greatly from the corresponding quantity for the case neglecting gravity. However, the general features of the theoretical seismograms for the two cases do not show any appreciable discrepancy. This means that the differences between the Common Spectrum for these cases may be cancelled during the process of summation of the contributions from the various modes.

2. Frequency Equation and Non-dimensional Frequency

It is assumed that:

1. The sphere is homogeneous
2. The spheroidal oscillation is considered
3. The radial component of stress is applied to a circular area around the pole
4. The effect of gravity is included.

Hereafter, the present case will be referred to as case (B) and the case neglecting gravitational effect as case (A). The displacement on the surface is expressed as

$$(u, v, w)=\frac{1}{2\pi}\int_{-\infty}^{\infty}(u(p), v(p), w(p)) \exp(jpt)dp\,, \tag{2.1}$$

in which

$$\left.\begin{aligned} u(p)&=\sum_{m,n}(U_n(r)/E)\cdot P_n^m(\cos\theta)\cdot \quad (C_{mn}\cos m\varphi + C'_{mn}\sin m\varphi)\cdot f^*(p)\,,\\ v(p)&=\sum_{m,n}(V_n(r)/E)\cdot\frac{d}{d\theta}P_n^m(\cos\theta)\cdot(\qquad\qquad\quad''\qquad\qquad)\cdot f^*(p)\,,\\ w(p)&=\sum_{m,n}(mV_n(r)/E)\cdot\frac{P_n^m(\cos\theta)}{\sin\theta}\cdot(-C_{mn}\sin m\varphi + C'_{mn}\cos m\varphi)\cdot f^*(p)\,. \end{aligned}\right\} \tag{2.2}$$

C_{mn} and C'_{mn} are the coefficients of spherical surface harmonics determined

by the geographical distribution of the applied force, $f^*(p)$ is the Fourier transform of the time function at the source and $P_n^m(\cos\theta)$ the associated Legendre function by Ferrers' definition.

$U_n(r)$ and $V_n(r)$ are functions giving the radial distribution of the displacement components and are expressed

$$\left.\begin{aligned} U_n(r)&=R\left[\frac{a}{k}j_{n+1}(k\zeta)-\frac{an}{k^2\zeta}\{1+(n+1)(M(k)-1)\}j_n(k\zeta)\right]\\ &\quad+S\left[\frac{a}{q}(L(q)-1)j_{n+1}(q\zeta)-\frac{na}{q^2\zeta}(L(q)+n)j_n(q\zeta)\right]+T\cdot n\zeta^{n-1},\\ V_n(r)&=R\left[\frac{a}{k}(M(k)-1)j_{n+1}(k\zeta)-\frac{a}{k^2\zeta}\{1+(n+1)(M(k)-1)\}j_n(k\zeta)\right]\\ &\quad+S\left[\frac{a}{q}j_{n+1}(q\zeta)-\frac{a}{q^2\zeta}(L(q)+n)j_n(q\zeta)\right]+T\cdot\zeta^{n-1} \end{aligned}\right\} \tag{2.3}$$

where $$\zeta=r/a\,.$$

The coefficients R, S, T and E are determined from the boundary conditions on the surface for the continuity of the stress components, and of the gravitational potential and its derivatives. These coefficients may be represented by the expressions

$$\left.\begin{aligned} &R=a_{22}\ a_{33}\ -a_{23}\ a_{32}\,,\quad S=-a_{21}\ a_{33}\ +a_{23}\ a_{31}\,,\\ &T=a_{21}\ a_{32}\ -a_{22}\ a_{31}\,, \end{aligned}\right\} \tag{2.4}$$

$$E=\begin{vmatrix} a_{11} & a_{12} & a_{13}\\ a_{21} & a_{22} & a_{23}\\ a_{31} & a_{32} & a_{33} \end{vmatrix}, \tag{2.5}$$

where a_{ij} can be written

$$\left.\begin{aligned} a_{11}&=\left(\frac{\lambda}{\mu}+2\right)\cdot j_n(k)+2\left[\{1+(n+1)(M(k)-1)\}\cdot\frac{n(1-n)}{k^2}\cdot j_n(k)\right.\\ &\quad\left.+\left\{\frac{n}{k}(1+(n+1)(M(k)-1))-\frac{n+2}{k}\right\}\cdot j_{n+1}(k)\right],\\ a_{12}&=\frac{\lambda}{\mu}(L(q)-1)\cdot j_n(q)+2\left[\left\{(L(q)+n)\frac{n(1-n)}{q^2}+L(q)-1\right\}\cdot j_n(q)\right.\\ &\quad\left.+\{-2(L(q)-1)+n(n+1)\}\cdot j_{n+1}(q)/q\right],\\ a_{13}&=2n(n-1)/a\,, \end{aligned}\right\}$$

$$
\left.\begin{aligned}
a_{21}&=(M(k)-1)\cdot j_n(k)+\frac{2(1-n)}{k^2}\{1+(n+1)(M(k)-1)\}\cdot j_n(k)\\
&\quad+\frac{2}{k}(2-M(k))\cdot j_{n+1}(k)\,,\\
a_{22}&=\left\{2(L(q)+n)\frac{1-n}{q^2}+1\right\}\cdot j_n(q)+\frac{2}{q}(L(q)-2)\cdot j_{n+1}(q)\,,\\
a_{23}&=2(n-1)/a\,,\\
a_{31}&=-4\pi\gamma\rho a\cdot\frac{n+1}{k^2}\{1-n(M(k)-1)\}\cdot j_n(k)\,,\\
a_{32}&=-4\pi\gamma\rho a\cdot\frac{n+1}{q^2}(L(q)-n-1)\cdot j_n(q)\,,\\
a_{33}&=(\Gamma n-p^2)(2n+1)-4\pi\gamma\rho n\,.
\end{aligned}\right\}\tag{2.6}
$$

In (2.3) and (2.6), $j_n(x)$ is the spherical Bessel function and

$$
\left.\begin{aligned}
&\left.\begin{matrix}2q^2\\2k^2\end{matrix}\right\}=a^2[\beta^2p^2+\alpha^2(p^2+4\Gamma)\pm\sqrt{(\beta^2p^2-\alpha^2(p^2+4\Gamma)^2)^2+4n(n+1)\alpha^2\beta^2\Gamma^2}]\,,\\
&\beta^2=\rho/\mu\,,\qquad\alpha^2=\rho/(\lambda+2\mu)\,,\\
&L(q)=1+\frac{\Gamma n(n+1)}{p^2+4\Gamma-q^2/(\alpha a)^2}\,,\qquad M(k)=1+\frac{\Gamma}{p^2-k^2/(\beta a)^2}\,,\\
&\Gamma=\frac{4}{3}\pi\gamma\rho\,.
\end{aligned}\right\}\tag{2.7}
$$

The integration of (2.1) can be evaluated by contour integration. As noted previously[3] the entire contribution may be found from the residues, which give the results

$$
\left.\begin{aligned}
u&=\frac{j}{2}\sum_{m,n,i}P_n^m(\cos\theta)\cdot(C_{mn}\cos m\varphi+C'_{mn}\sin m\varphi)\cdot\\
&\quad\times\left[\frac{U_n(r)}{dE\ dp}\cdot f^*(p)\cdot\exp(jpt)\right]_{p=ip_n}\,,\\
v&=\frac{j}{2}\sum_{m,n,i}\frac{d}{d\theta}P_n^m(\cos\theta)\cdot(C_{mn}\cos m\varphi+C'_{mn}\sin m\varphi)\cdot\\
&\quad\times\left[\frac{V_n(r)}{dE\ dp}\cdot f^*(p)\cdot\exp(jpt)\right]_{p=ip_n}\,,
\end{aligned}\right\}\tag{2.8}
$$

where ${}_ip_n$ is the root of the frequency equation $E=0$. w has a similar expression.

In case (A) the non-dimensional frequency ($\eta=pa/V_S$) is a function of the ratio λ/μ only, while in case (B), as is seen from the expression (2.6), it is a complicated function of λ, μ, V_S, a and $\gamma\rho$. In the present study the following numerical values are assumed.

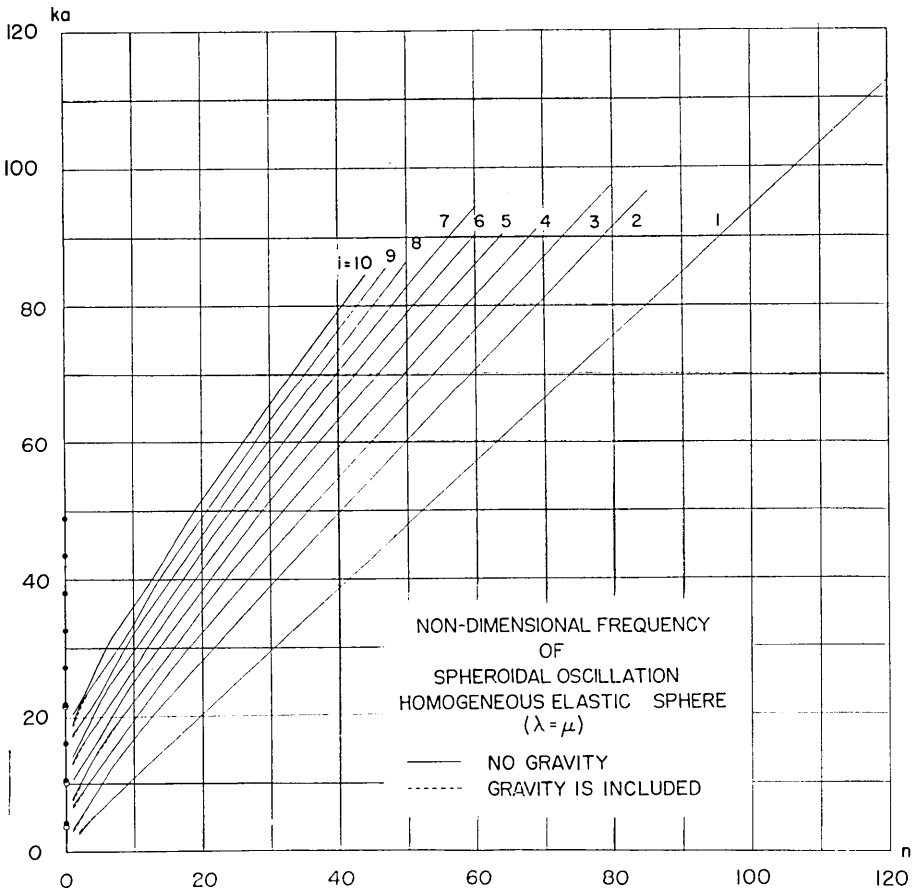

Fig. 1-A. Non-dimensional frequency ($ka=(2\pi a/V_s)/T$) of the spheroidal free oscillation for a homogeneous elastic sphere. Solid curve and solid circle refer to the case without gravity, and broken curve and open circle to the case of a gravitating sphere.

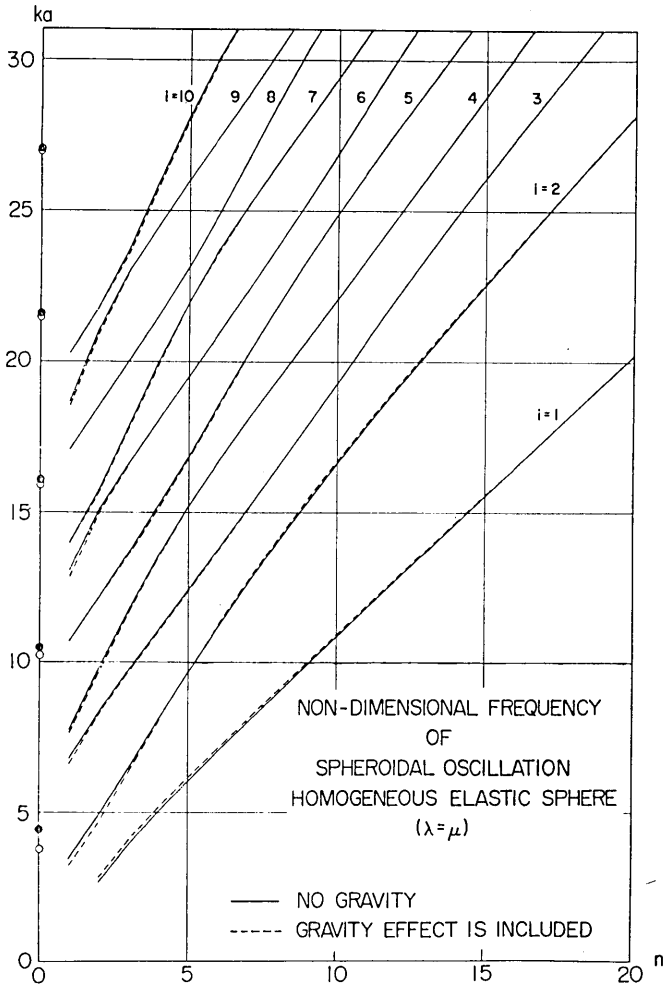

Fig. 1-B. Enlargement of a part of Figure 1-A showing detailed features for smaller values of colatitudinal order number n.

$$\left.\begin{aligned} &a \quad \text{(radius of the earth)} = 6370\ \text{km} \\ &V_S \quad \text{(velocity of shear waves)} = 6.667\ \text{km/sec} \\ &V_P \quad \text{(velocity of dilatational waves)} = 11.55\ \text{km/sec} \\ &\lambda = \mu \\ &\rho \quad \text{(density)} = 5.52\ \text{gr/cm}^3 \\ &\gamma \quad \text{(gravitational constant)} = 6.67 \times 10^{-8}\ \text{c.g.s.} \\ &\Gamma = 154.2245 \times 10^{-8}\ \text{c.g.s.} \end{aligned}\right\} \qquad (2.9)$$

The non-dimensional frequency is calculated and is given in Figures 1–A and 1–B in the form of continuous curves. In the present study, additional computations were made for case (A) for the tenth radial mode ($i=10$) and for the fundamental mode for colatitudinal order numbers 95 through 160. The curve of non-dimensional frequency vs. order number for the fundamental mode can be almost linearly extrapolated up to $n=160$. Solid lines refer to case (A) and broken lines to case (B). The difference between the non-dimensional frequencies for these two cases becomes smaller as the colatitudinal order number n increases. Figure 1 shows also that the non-dimensional frequency (period) of the fundamental mode of case (B) is larger (smaller) than the corresponding value of case (A). In order to show detailed features, a part of Figure 1–A is drawn in magnified scale in Figure 1–B.

When $n=0$, that is the case in which simple expansion and contraction repeats alternately, the non-dimensional frequency will be given by solving the equation of motion[4]

$$\frac{d^2u}{dr^2}+\frac{2}{r}\frac{du}{dr}-\frac{2}{r^2}u+\frac{\rho(p^2+4\Gamma)}{\lambda+2\mu}u=0\,, \tag{2.10}$$

under the condition on the surface that

$$(\lambda+2\mu)\frac{du}{dr}+4\mu\frac{u}{r}=0\,. \tag{2.11}$$

The non-dimensional frequency thus obtained is smaller than that of case (A) and they are related by the expression

$$\eta_{(B)}^2+\frac{4a^2\Gamma}{V_S{}^2}=\eta_{(A)}^2 \tag{2.12}$$

When $n\geqq 1$, the effect of gravity in the three coupled equations of motion[4] appears on both sides of these equations. It not only serves to reduce the frequency as for the case of pure dilatation, above, but also enters as terms which make the frequency larger and thus makes the relation between the frequencies for cases (A) and (B) complicated. Further study of this point will be the subject of future investigations.

3. Phase and Group Velocities

Phase and group velocities are calculated by the asymptotic formulae

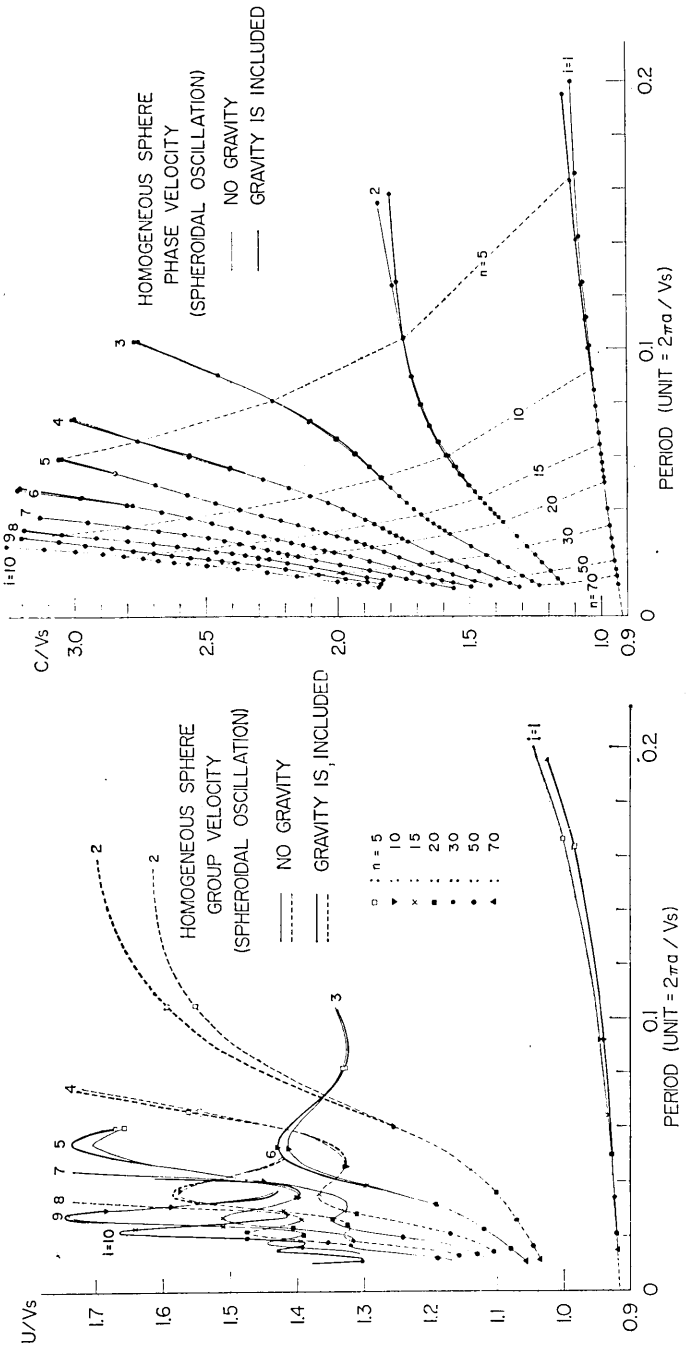

Fig. 2. Relation of phase and group velocities to period. Thin curves refer to the non-gravitating case and thick curves to the gravitating case.

$$C=V_S\cdot\eta/(n+1/2)\,, \tag{3.1}$$

and

$$U=V_S\cdot d\eta/dn\,. \tag{3.2}$$

The results are given in Figure 2 which also shows the results for case (A). In Figure 2, thick lines refer to the case (B) and thin lines to the case (A). The difference between the two cases is small except for the fundamental mode and for the first higher radial mode for small values of colatitudinal order number n. For the fundamental mode, the phase velocity for case (B) —with gravity— is larger than that for case (A), while the group velocity for case (B) is smaller.

4. Common Spectrum

The radial and colatitudinal components of the Common Spectrum, as defined in our previous paper,[5] are given in Figure 3, in the form of continuous curves. A part of the figure is shown in a magnified scale to show detailed features. The spectral values of the radial-component for $n=0$ are given by solid circles, which correspond to the solid circles in Figure 1. In Figure 3, the Common Spectrum of case (B) is given by thick lines and the values for case (A) appear as thin lines. The difference between these two cases is not very great, but the difference for the colatitudinal component is much larger than that found for the radial component. The results for the fundamental mode for orders larger than 100 are given in another enclosure.

5. Theoretical Seismograms

Axial symmetry ($m=0$) is assumed in the following numerical computations. The spatial and temporal distributions of the applied force are assumed to be the same as for case (A), without gravity. Thus the spatial distribution is

$$\Phi(\theta,\varphi)=\Phi^0(\cos\theta)=\begin{cases}1 & \theta<\theta_0\\ 0 & \theta>\theta_0\,,\end{cases} \tag{5.1}$$

and the time function is

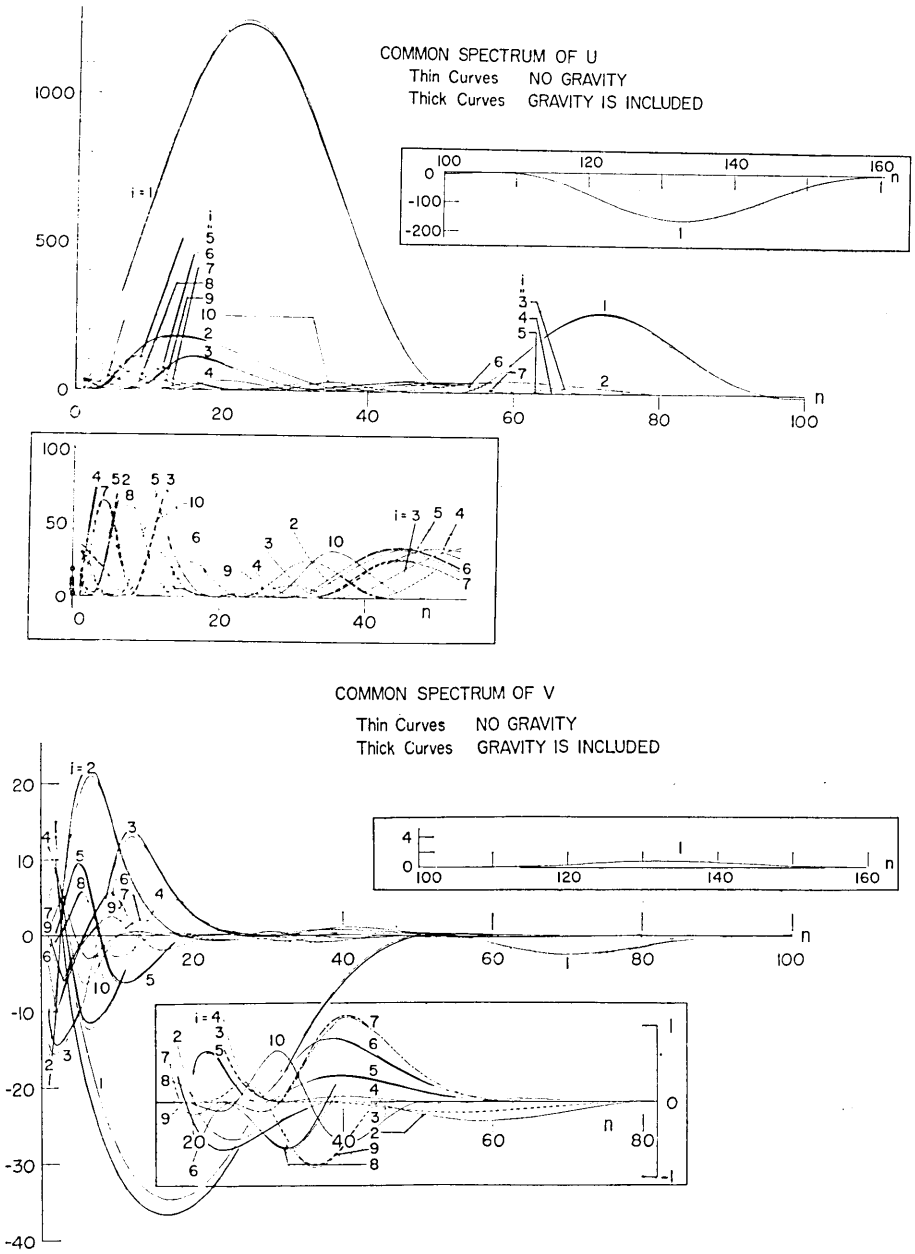

Fig. 3. Common Spectrum of radial and colatitudinal components of the disturbance. Curves for the fundamental mode in enclosure. To show the features of the curves clearly, part of the figure is shown in magnified scale in another enclosure. Thin and thick curves correspond to the case of non-gravitating and gravitating sphere respectively.

$$f(t)=\begin{cases}-1 & -t_1<t<0\\ 1 & 0<t<t_1\\ 0 & |t|>t_1\end{cases}, \tag{5.2}$$

from which there results

$$f^*(p)=-4j\sin^2(pt_1/2)/p\,. \tag{5.3}$$

The numerical values assumed are

$$\theta_0=0.04 \text{ radian},$$
$$t_1=0.02 \text{ (unit}=2\pi a/V_S)\,. \tag{5.4}$$

The largest values of colatitudinal order number $n_{\max}$ employed for each of the radial modes are[6]

$i=$	1	2	3	4	5	6	7	8	9	10
$n_{\max}=$	160	79	73	69	64	60	60	39	44	54

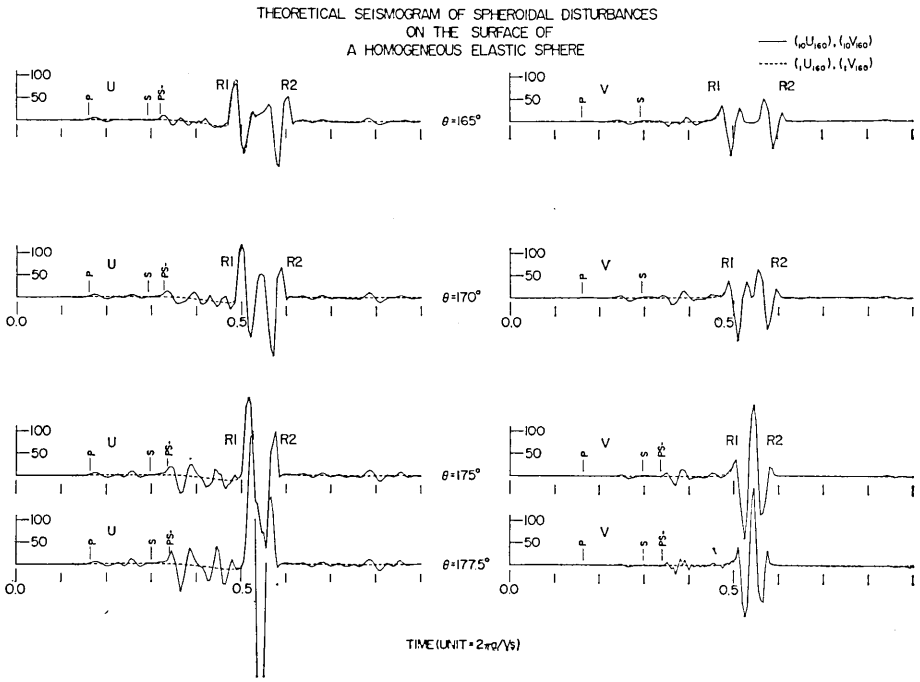

Fig. 5. Theoretical seismograms showing the change of wave pattern near the antipode. Notation and unit of ordinate scale are the same as those in Figure 4.

Theoretical seismograms were calculated at three points on the surface for epicentral distances $\theta=30°$, $90°$, $150°$ and the results are shown in Figure 4. In this figure, the solid lines imply $({}_{10}u_{160})$ and $({}_{10}v_{160})$ and broken lines refer to $({}_{1}u_{160})$ and $({}_{1}v_{160})$, where the parentheses mean:

$$({}_{i}u_{n})=\sum_{i=1}^{i}\sum_{n=0}^{n}{}_{i}u_{n}\,,\qquad ({}_{i}v_{n})=\sum_{i=1}^{i}\sum_{n=0}^{n}{}_{i}v_{n}\,. \tag{5.5}$$

Expected arrivals of the various body phases calculated from the simple theory of geometrical optics are indicated by the arrows in Figure 4. The travel time curves for these body waves are found in an earlier report.[7)]

The theoretical seismograms are quite similar for the cases (A) and (B) except that there are slight differences during the passage of the body waves. This implies that the effect of gravity is negligibly small for most arrivals displayed by the theoretical seismograms. Figure 5 was prepared to show changes in the wave pattern near the antipode. Since waves such as the surface waves (and the *PS*-waves) converge towards the pole or the antipode, the amplitudes of these waves increases rapidly as they approach the antipode. By contrast, *P* and *S* waves which arrive at the antipode directly from the origin do not show any change in amplitude near the antipode.

The numerical computations were carried out on an IBM 7090 through the project UNICON to which our sincere thanks are due.

References

1) Y. SATÔ, T. USAMI and M. EWING, "Basic Study on the Oscillation of a Homogeneous Elastic Sphere IV. Propagation of Disturbances on the Sphere," *Geophys. Mag.*, **31** (1962), 237–242.

Y. SATÔ, T. USAMI, M. LANDISMAN and M. EWING, "Basic Study on the Oscillation of a Sphere Part V: Propagation of Torsional Disturbances on a Radially Heterogeneous Sphere. Case of a Homogeneous Mantle with a Liquid Core," *Geophys. J.*, **8** (1963), 44–63.

T. USAMI and Y. SATÔ, "Propagation of Spheroidal Disturbances on a Homogeneous Elastic Sphere," *Bull. Earthq. Res. Inst.*, **42** (1964), 273–287.

Y. SATÔ and T. USAMI, "Propagation of Spheroidal Disturbances on an Elastic Sphere with a Homogeneous Mantle and a Core," *Bull. Earthq. Res. Inst.*, **42** (1964), 407–425.

T. USAMI, Y. SATÔ and M. LANDISMAN, "Theoretical Seismograms of Spheroidal Type on the Surface of a Heterogeneous Spherical Earth," *Bull. Earthq. Res. Inst.*, **43** (1965), 641–660.

M. LANDISMAN, Y. SATÔ and T. USAMI, "Propagation of Disturbances in a Gutenberg-

THEORETICAL SEISMOGRAM OF SPHEROIDAL DISTURBANCES
ON THE SURFACE OF A HOMOGENEOUS ELASTIC SPHERE
(GRAVITY EFFECT IS INCLUDED)

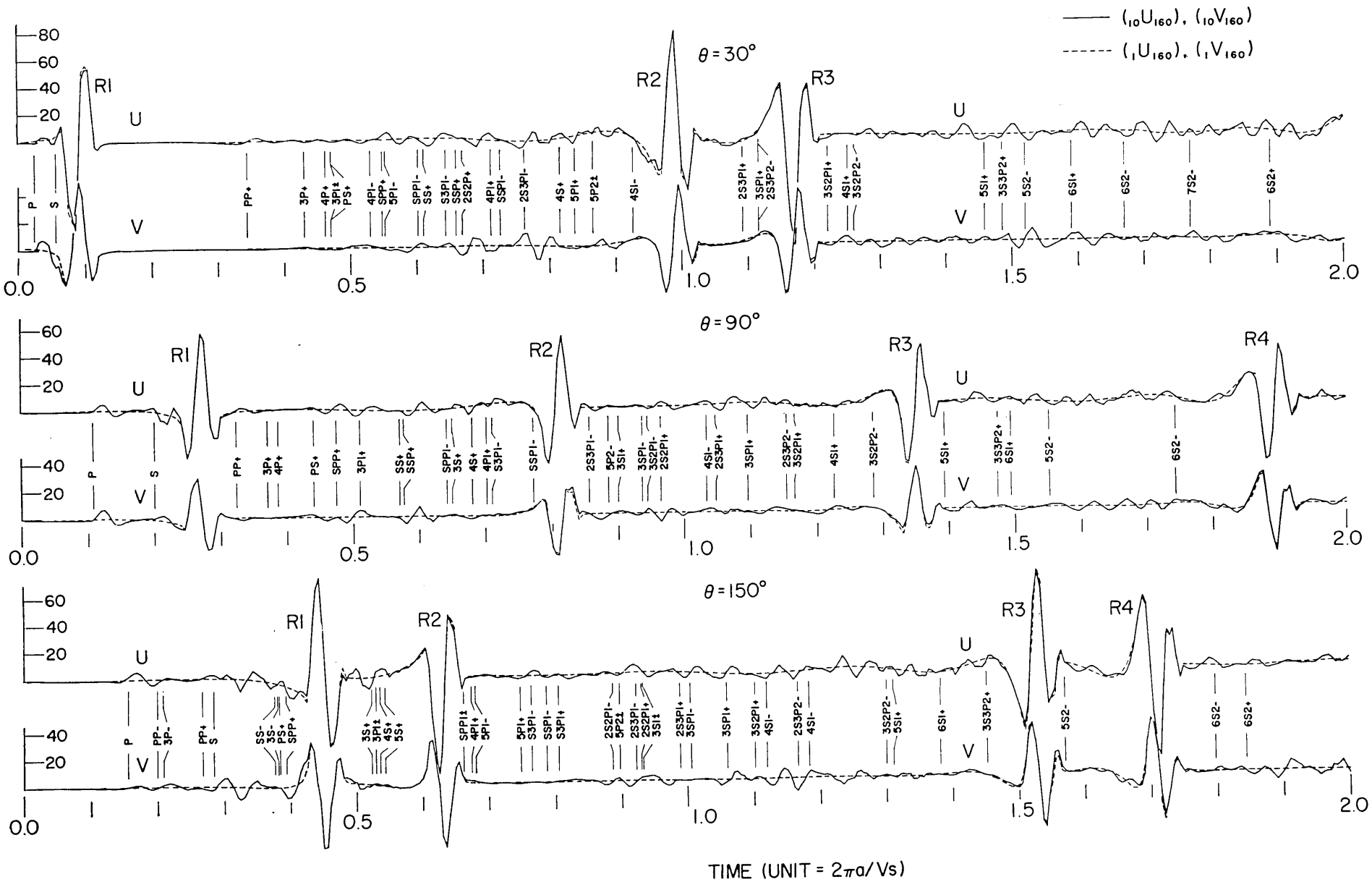

Fig. 4. Theoretical seismogram of radial and colatitudinal displacements at epicentral distances θ=30°, 90° and 150° caused by a radial stress applied to a circular area around the pole. Arrows show the arrival times of various phases of body waves calculated by the theory of geometrical optics. Solid line refers to $({}_{1C}u_{160})$ and $({}_{10}v_{160})$ and broken line to $({}_{1}u_{160})$ and $({}_{1}v_{160})$. Unit of time is $2\pi a/V_S$, where a and V_S are the radius and shear velocity of the sphere. The labels nPmS imply PP... PPSS...SS, for multiple reflections which travel n times as P and m times as S. $k+$ at the end of the labels means an epicentral distance equal to $2\pi(k+1)-\theta$ radians and $k-$ means an epicentral distance of $2k\pi+\theta$ radians.

Bullen A′ Spherical Earth Model: Travel Times and Amplitudes of S Waves," *American Geophysical Union Monograph No. 10* (1966), in press.
2) Third paper of 1).
3) First paper of 1).
4) C. L. PEKERIS and H. JAROSCH, "The Free Oscillation of the Earth," in "Contributions in Geophysics" (*Gutenberg Volume*), *Intern. Ser. Monographs Earth Sci., 1,* (Pergamon Press, London, 1958), pp. 171-192.
5) Third paper of 1).
6) Last paper of 1).
7) Third paper of 1).

---

42. 等質等方弾性球の表面を伝わるスフェロイド型振動

——重力の影響を考えた場合——

地震研究所 宇佐美龍夫
佐藤泰夫

1. 筆者らが従来行って来た弾性球を伝わる擾乱の理論地震記象の研究では重力を考慮しなかった．今回は，重力が振動周期，位相及群速度，コモン・スペクトルおよび理論地震記象におよぼす影響をしらべる手初めとして，重力均衡下にある等質等方弾性球を伝わるスフェロイド型擾乱について計算した．

2. 固有周期は λ, μ, (ラメ定数), ρ (密度), a (地球の半径), r (万有引力の常数) の複雑な函数となるので，モデルをはっきり決める必要がある．次の値を採用した．a=6370 km, V_S=6.667 km/sec, V_P=11.55 km/sec, ρ=5.52 gr/cm^3, $r=6.67\times10^{-8}$ c.g.s.

3. 固有振動の周波数について次のことが分った．$n=0$ の時には i のいかんにかゝわらず重力が加わると周波数は小さくなる．$i=1$ で $n\geqq1$ の時には周波数は重力がない場合よりも大きくなる．その他のモードについては，重力の影響は複雑である，しかし n が大きくなるにしたがって，重力の影響は小さくなり，$n=20\sim40$ 以上ではほとんど無視できる．

4. 位相速度・群速度に及ぼす重力の影響は小さい．

5. コモン・スペクトルは，半径方向の成分については重力の影響は小さいが，緯度方向の成分については無視できない．しかしこれが v 成分の理論地震記象に影響を及ぼさないのは，個々のモードに対する重力の影響がお互いに打ち消し合うからであろう．

6. 理論地震記象の計算に当っては，軸対称 ($m=0$) を仮定した．外力としては極のまわりに次のような半径方向の力だけが作用すると考えた．

$$\Phi(\theta,\varphi)=\Phi^0(\cos\theta)=\begin{cases}1 & \theta<\theta_0\\ 0 & \theta>\theta_0\end{cases}\qquad(\theta_0=0.04\ \text{ラヂアン})$$

$$f(t)=\begin{cases}-1 & -t_1<t<0\\ 1 & 0<t<t_1\\ 0 & t_1<|t|\end{cases}\qquad(t_1=0.02)$$

時間の単位としては (周長)/(S 波速度) を採用した．計算の方法は従来と同じで，変位を自由振動の各モードの和として表わした．

7. 理論地震記象は重力のない場合によく似ている．実体波の部分に，僅かの違いが見られる程度である．また，極付近での波の伝わり方を示すために，極付近の理論地震記象を計算した．